Journal of Robotics and Control (JRC)
Volume 3, Issue 5, September 2022
ISSN: 2715-5072, DOI: 10.18196/jrc.v3i5.15326

Synchronous Reluctance Motor Performance Improvement Using MTPA Control Strategy and Five-Level Inverter Topology

Yassine Zahraoui [1*], Mohamed Moutchou [1], Souad Tayane [1], Chaymae Fahassa [2], Sara Elbadaoui [2], Alfian Ma'arif [3]
[1] Electrical Engineering Department, Higher National School of Arts and Crafts, Hassan II University, Casablanca 20670, Morocco
[2] Electrical Engineering Department, Mohammadia School of Engineering, Mohammed V University, Rabat 765, Morocco
[3] Universitas Ahmad Dahlan, Yogyakarta, Indonesia
Emails: [1] yassine.zahraoui1-etu@etu.univh2c.ma, mohamed.moutchou@univh2c.ma, souad.tayane@univh2c.ma, [2] fahassa.chaymae@gmail.com, sara_elbadaoui@um5.ac.ma, [3] alfian.maarif@te.uad.ac.id
*Corresponding Author

***Abstract*—An improved vector control method is presented in this study to enhance synchronous reluctance motor (SynRM) performance. The maximum torque per ampere (MTPA) technique has demonstrated good dynamic properties since the torque control is closely tied to the current control. The selection of the control approach is primarily influenced by how the reference current values will be defined. Additionally, a five-level neutral-point-clamped (NPC) inverter replaces the traditional two-level inverter. Only eight voltage vectors can be produced by a two-level inverter, whereas one hundred twenty-five voltage vectors can be generated by a five-level inverter. The goal is to produce an output voltage vector that closely resembles the reference voltage vector in order to ensure a quick response on the one hand and enhance dynamic performance on the other. An exact comparison of the suggested vector control strategy's properties is made once it has been simulated in MATLAB/Simulink. The acquired findings are satisfactory and high performance is attained in terms of response time, torque ripple reduction, and current waveform improvement.**

***Keywords*—Synchronous reluctance motor; Performance improvement; MTPA control strategy; Five-level inverter topology; Ripples reduction**

I. Introduction

Electric machines are now required to be more efficient and small, and there are several solutions available to meet this goal [1]. Due to their many benefits, such as their high power density (15kW/L) and high efficiency (>95%), machines exploiting rare heaps of the earth (PMSM, for instance) are frequently the technological solutions used [2]. However, the realities and limitations of the market for rare piles of earth drive businesses to develop palliative measures that are less expensive and economically hazardous. The paper will therefore examine synchronous reluctance machines as a substitute technology in this setting [3].

Thus, stepper control [4] or vector control [5] have been used to design high-efficiency synchronous reluctance motors for high-power industrial applications [6]. It was discovered that the torques seen in these motors retain significant fluctuations and produce noise, preventing their usage for air conditioning or other applications that might benefit the general public [7].

There are a lot of negative aspects of SynRM. The rotor's salience, which is where the electromagnetic torque originates, generates ripples on it, which can cause vibrations and acoustic noise [8] [9]. This sort of equipment has a poor power factor, which causes the inverter to be oversized [10]. Additionally, it is quite susceptible to magnetic saturation, which significantly affects the average torque created [11]. The major goal of this research is to create a vector control optimization approach to boost SynRM's performance, particularly in terms of efficiency [12].

As seen by a significant number of recent articles, developing optimization techniques at the control level in order to improve SynRM performance is still a hot topic [13], [14], [15], [16], [17], [18]. The textile sector, machine tools, and applications requiring fast rotating speeds are the current application areas for SynRM. It is currently employed in applications for traction, electric vehicles, pumping, and ventilation [19].

Standard pulse width modulation (PWM) is typically used to regulate two-level inverters, although this relationship does not eliminate harmonics in the inverter output voltage [20], [21]. These harmonics are reduced by the three PWM-based carriers in the five-level NPC structure, which also ensures a constant switching frequency.

II. State-space mathematical model of SynRM

The dynamic model of the SynRM, which is defined by the electrical and mechanical characteristics and describes the electromagnetic and electromechanical processes, must be understood in order to regulate the SynRM's variable speed [22]. The classical model based on the Park transformation complies with the following presumptions, according to [23]:

- The magnetic circuits' hysteresis is minimal;
- There is an unsaturated magnetic circuit;
- Gap harmonics are not considered;
- The air gap's sinusoidal spatial distribution of the magneto-motive forces;
- The influence of temperature on the value of the resistors is disregarded.

The synchronous reluctance motor's electrical equations in the d-q reference frame are:

$$\begin{bmatrix} v_{ds} \\ v_{qs} \end{bmatrix} = R_s \begin{bmatrix} i_{ds} \\ i_{qs} \end{bmatrix} + \begin{bmatrix} L_d \\ L_q \end{bmatrix} \frac{d}{dt} \begin{bmatrix} i_{ds} \\ i_{qs} \end{bmatrix} + p\Omega \begin{bmatrix} 0 & -L_q \\ L_d & 0 \end{bmatrix} \begin{bmatrix} i_{ds} \\ i_{qs} \end{bmatrix} \quad (1)$$

The d-q reference frame's current components are i_{ds} and i_{qs}. Stator voltage components include v_{ds} and v_{qs}. Stator resistance is denoted by R_s. The direct and quadrature axes' inductances are denoted by L_d and L_q. The pole pair number is p, and Ω is the mechanical speed. An expression for the electromagnetic torque is:

$$T_{em} = \frac{3}{2} p (L_d - L_q) i_{ds} i_{qs} \quad (2)$$

The total flux through the windings d and q in the rotor-related frame is denoted by:

$$\begin{cases} \phi_{ds} = L_d i_{ds} \\ \phi_{qs} = L_q i_{qs} \end{cases} \quad (3)$$

hence

$$\begin{cases} v_{ds} = R_s i_{ds} + \frac{d\phi_{ds}}{dt} - p\Omega\phi_{qs} \\ v_{qs} = R_s i_{qs} + \frac{d\phi_{qs}}{dt} + p\Omega\phi_{ds} \end{cases} \quad (4)$$

with

$$\phi_s = \sqrt{\phi_{ds}^2 + \phi_{qs}^2} \quad (5)$$

and

$$\tan\delta = \frac{i_{qs}}{i_{ds}} \quad (6)$$

Following (2), the torque equation is:

$$T_{em} = p(\phi_{ds} i_{qs} - \phi_{qs} i_{ds}) \quad (7)$$

The rotor motion is described as follows:

$$J\frac{\Omega}{dt} = T_{em} - T_l - f\Omega \quad (8)$$

Where f is the friction coefficient, T_l is the load torque, and J is the motor inertia. The product between the current and the mechanical speed on the one hand, and between the current and its derivative on the other, are the terms of non-linearity in the synchronous reluctance motor model in (1) [24], [25]. The vector diagram of the steady-state synchronous reluctance motor is shown in Fig. 1.

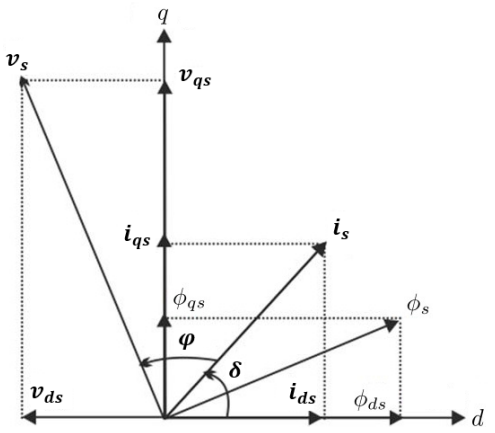

Fig. 1: Steady-state vector diagram of the SynRM

III. Optimal currents calculation for the MTPA strategy

A. Constant Current Angle Control

In order to indirectly control the i_{ds} and i_{qs} stator current components in the d-q reference frame, one must manipulate the SynRM torque. However, a degree of freedom permits maximizing a second criterion because the torque is proportional to the product $i_{ds} \times i_{qs}$ (efficiency, speed range, power factor, etc.). As a result, there are as many control strategies as there are criteria. The vector control law comprises a loop for speed regulation in addition to two current loops, one for each axis [26], [27].

The present loops are on the first level. These loops regulate the stator current d-q components to maintain steady-state signal stability. The anti-windup controller rejects the electromotive force that connects the two axes (d and q) and provides zero static error [28].

The tangent of the current angle (δ), which is the angle between the current space vector and rotor-oriented d-axis stator current, is used to estimate the d and q-axis reference currents from the reference value of torque in the MTPA constant current angle control approach [29], [30]. Below is a quick explanation of the MTPA current angle control technique's estimation of the reference currents.

B. MTPA strategy

This approach ensures great performance at low speeds and during start-up [31]. You can express the electromagnetic torque as follows:

$$T_{em} = \frac{3}{2} p (L_d - L_q) i_{ds} i_{qs} = \frac{3}{2} p (L_d - L_q) i_s^2 sin(2\delta) \quad (9)$$

The greatest torque in absolute values is obtained for $\delta = \pm\frac{\pi}{4}$ for a certain current modulus i_s [32]. When we get i_{ds}=$|i_{qs}|$, the references of the currents are as follows:

$$i_{ds}^* = \frac{2T_{em}^*}{3p(L_d - L_q)} \quad (10)$$

and

$$i_{qs}^{*} = i_{ds}^{*} sign(T_{em}^{*}) \quad (11)$$

In order to attain the current limit $i_{ds_{max}}$ at point P_1, which corresponds to the maximum torque, the current increases in a 45° direction from point O [33]. The current limits on the d and q axes, i_{ds_1} and i_{qs_1} thus result in:

$$i_{ds_1} = i_{qs_1} = \frac{\sqrt{2}}{2} i_{s_{max}} \quad (12)$$

The MTPA control strategy's trajectory is depicted in Fig. 2.

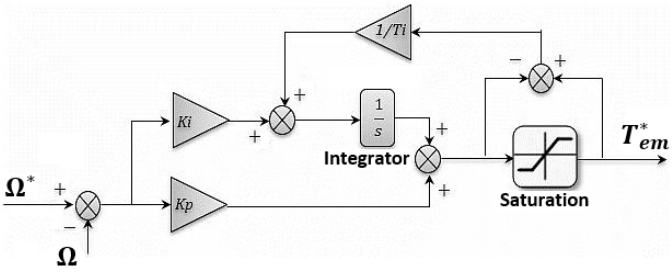

Fig. 3: Structure of the proposed anti-windup controller.

IV. Anti-windup controller for speed loop regulation

Generally, proportional-integral (PI) regulators are utilized for automation control. This is done by juxtaposing the speed reference cue to the real computed speed signal. Afterward, the juxtaposition error will be the PI controller input. PI controllers generally ignore the physical limitations of the system, such as maximal current, and voltage. The PI controller used in this research is the anti-windup regulator. This makes it possible to ameliorate the performance of the speed control by annulling the windup fact caused by the saturation of the neat integrator [34]. Fig. 3 displays the block diagram of the suggested anti-windup speed controller.

This strategy incorporates correcting the integral action according to the differentiation between the control signal and the saturation boundary. The difference is transmitted to a gain block (pursuing time constant T_i) before returning to the integrator. Each anti-windup controller has three tuning gains; their values are determined by trial and error. This technique consists of performing repetitive tests and tuning each gain separately from the others to view its effect.

V. Five-level NPC inverter design

A. Main topology

Fig. 4 depicts the general structure of the five-level NPC inverter. Three symmetrical arms make up this arrangement, and each arm has eight bidirectional switches mounted in series. To prevent a short-circuit of the inverter input continuous voltage, these switches must not be opened or closed at the same time [35].

A bi-controllable semiconductor S_{ij} (i=A, B, C and j=1,…, 8) and a diode placed in anti-parallel make up each switch. Ten floating diodes per arm D_k (k=1, …, 10) are used to ensure the application of various voltage levels at each arm's output [36].

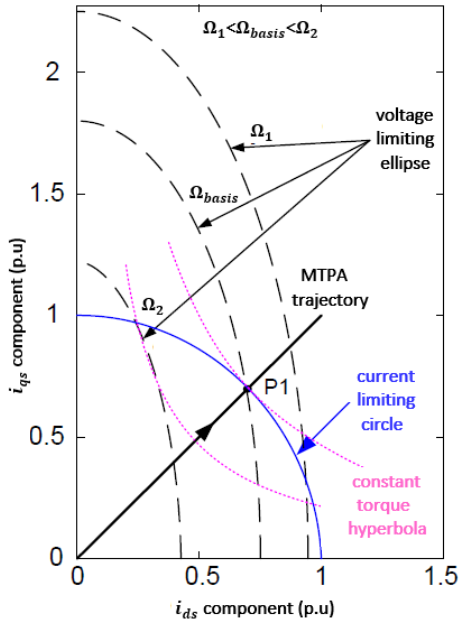

Fig. 2: MTPA control trajectory

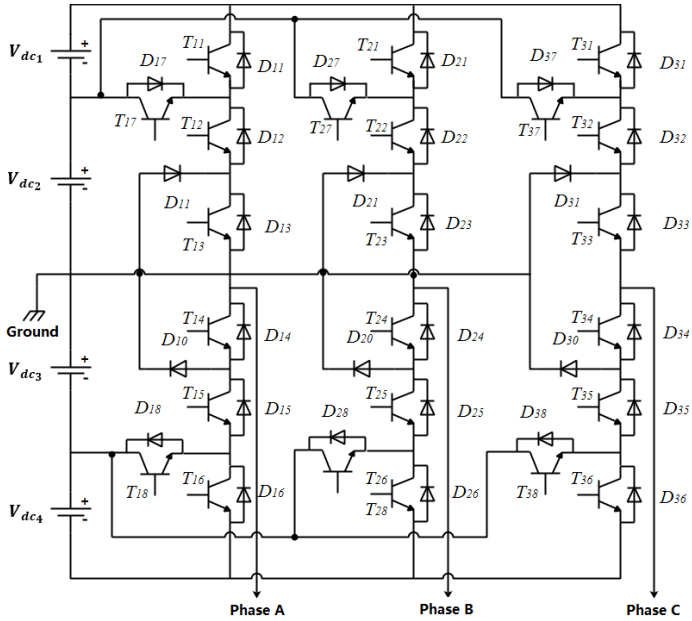

Fig. 4: The structure of the five-level NPC inverter.

Because it provides five different voltage levels per arm– $\frac{+V_{dc}}{2}$, $\frac{+V_{dc}}{4}$, 0, $\frac{-V_{dc}}{4}$, $\frac{-V_{dc}}{2}$–this inverter is known as a five level inverter.

Seven different voltage levels can be applied to the same phase by combining the twelve switches on the same arm:

$$\begin{cases} (1,1,1,1,0,0,0,0) \rightarrow +\frac{V_{dc}}{2} \\ (1,1,1,0,1,0,0,0) \rightarrow \ \ +\frac{V_{dc}}{4} \\ (1,1,0,0,1,1,0,0) \rightarrow 0 \\ (1,0,0,0,1,1,1,0) \rightarrow \ \ -\frac{V_{dc}}{4} \\ (0,0,0,0,1,1,1,1) \rightarrow -\frac{V_{dc}}{2} \end{cases} \tag{13}$$

In contrast to the two-level inverter, which can only supply eight voltage vectors, this results [37]. According to Fig. 5, the seven-level NPC inverter can generate one hundred twenty-five voltage vectors [38].

The output voltage vector's one hundred twenty-five positions divide the vector diagram into six triangular sections. Thirty-six triangular regions make up each sector. As a result, the entire vector diagram contains two hundred sixteen triangular sections.

For many system applications, multilevel inverters are a good option, particularly for drive systems. This is due to the several benefits they offer, including reduced total harmonic distortion (THD) and improved power factor [39].

B. PWM strategy

Multilevel converter control techniques are an extension of two-level converter control strategies. Over the past two decades, a number of triangular-sinusoidal multilevel converter approaches have been researched.

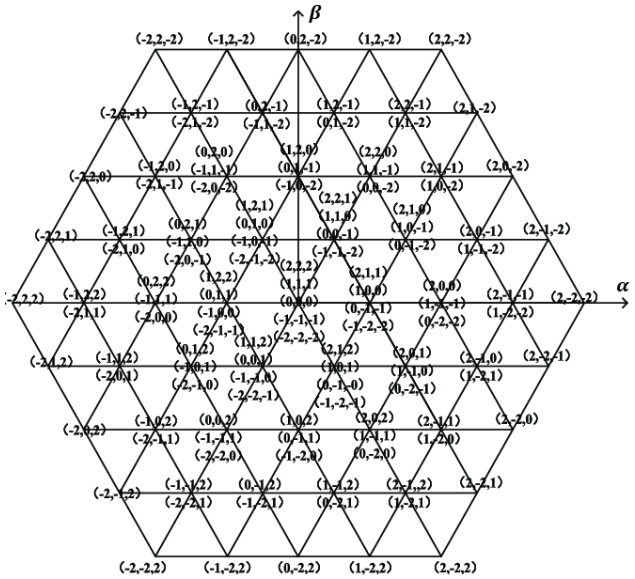

Fig. 5: Space vector diagram of the provided voltage vectors by the five-level NPC inverter.

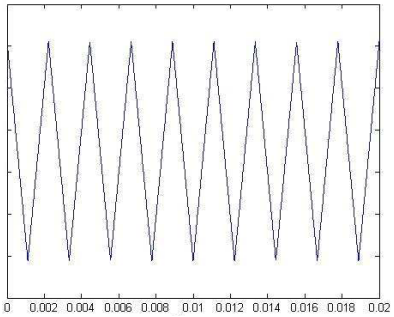

(a) Symmetrical triangles

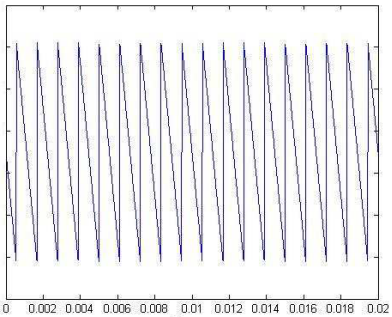

(b) Saw-tooth leading edge

Fig. 6: Examples of triangular carriers

The carrier signal must be composed of line segments with equal slopes in order to have a linear adjustment characteristic. As depicted in Fig. 6, a contrast is drawn between the saw-tooth carriers and the symmetrical triangular carriers.

The advantage of the symmetrical triangles technique is that it permits sampling at a frequency that is twice as high as the carrier frequency, which produces a signal that is often of higher quality. Multilevel inverters often built on carriers with symmetrical triangles. The modulation approach is characterized by their arrangement [40], [41].

The modulated signal and the control signals are determined by the combination of the comparison signals. The converter produces the modulated signal via the control signals; it typically serves no purpose as a signal and frequently travels straight from the comparison signals to the converter's control signals [42].

In Fig. 7, the most common shapes are resumed: noitemsep,topsep=0pt

- In-phase carriers (Fig. 7(a)),
- Alternate carriers (Fig. 7(b)),
- In-opposition carriers (Fig. 7(c)).

The performance of the suggested five-level inverter, which is based on MTPA vector control, is improved in this research article using alternative carriers.

In Fig. 8, the proposed vector control scheme's block diagram including the multilevel NPC inverter, PWM modulation method, and anti-windup controllers is shown.

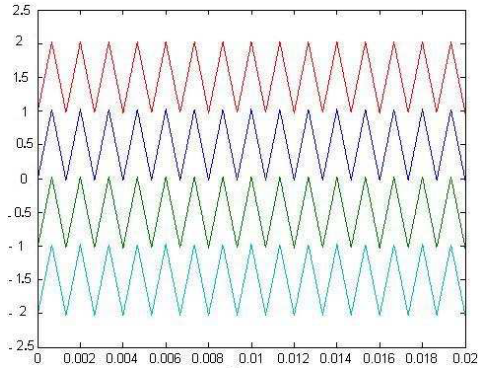

(a) In-phase carriers

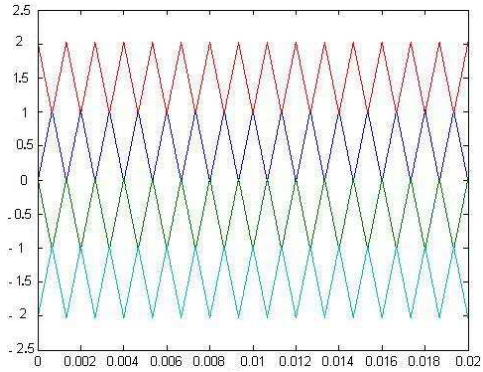

(b) Alternate carriers

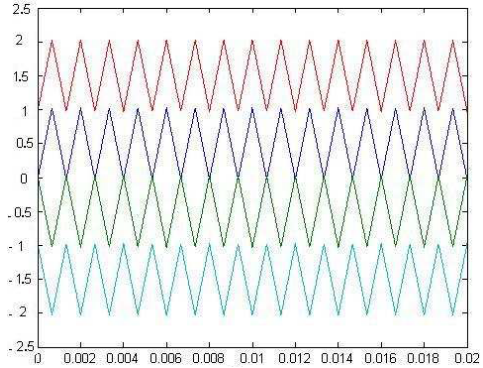

(c) In-opposition carriers

Fig. 7: Main carrier arrangements

VI. Simulation results and discussion

A. Simulation environment

The conventional technique and the suggested method are contrasted, emphasized, and discussed. The PWM controller uses alternate carriers, and four alternate carriers are commanding the five-level NPC inverter. The rated power and the parameters of the synchronous reluctance motor used in this simulation investigation are listed in Table I. The simulation results in a low-speed zone with load application are shown in Fig. 9. 5 N.m of load torque is suddenly applied at t_1=0.6s and removed at t_2=1.6s. The THD value of the electromagnetic torque is displayed in Fig. 10, and the THD value of the phase current is highlighted in Fig. 11.

TABLE I: Rated power and parameters of the machine used in the simulation

Rated power	1.1 kW
Rated speed	1500 tr/min
Rated voltage	220/380 V
Rated torque	7 N.m
Frequency	50 Hz
Pole pair number	2
Stator resistance	6.2 Ω
Apparent stator inductance L_d	0.34 H
Apparent stator inductance L_q	0.105 H
Inertia moment	0.08 $N.m.s^2$
Viscous friction coefficient	0.0001 N.m.s/rad

B. Results analysis

The two vector control techniques kept good dynamics when starting up, as shown in Figs. 9(a), and (b). The applied load is quickly rejected by the speed controller-based anti-windup action on the proposed scheme.

The proposed technique based on multilevel inverter has a quick response time comparing to the conventional technique. The transient response is fast because the anti-windup controller in the speed loop rejects the windup action caused by the saturation of the integrator.

The torque waveform in the proposed technique based on multilevel inverter in Fig. 9(d) is smoother than that of the conventional technique in Fig. 9(c). The torque ripples are reduced significantly. The more the inverter level is increased, the more the torque ripples are reduced.

The phase current waveform in the proposed technique based on multilevel inverter in Fig. 9(f) are smoother than that of the conventional technique in Fig. 9(e). The phase current ripples are then reduced. The more the inverter level is increased, the more the phase current ripples are reduced.

The d-q current components (i_{ds} and i_{qs}) waveform in the proposed technique based on multilevel inverter in Fig. 9(h) are smoother than that of the conventional technique in Fig. 9(g). The current's shape is improved significantly.

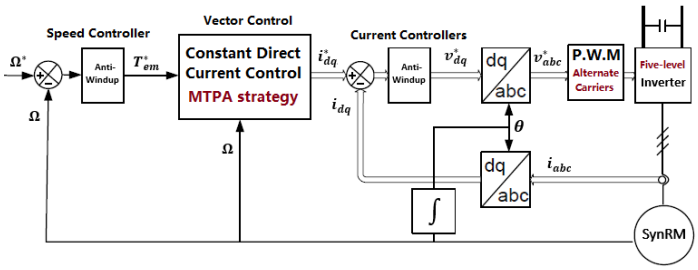

Fig. 8: The proposed control scheme.

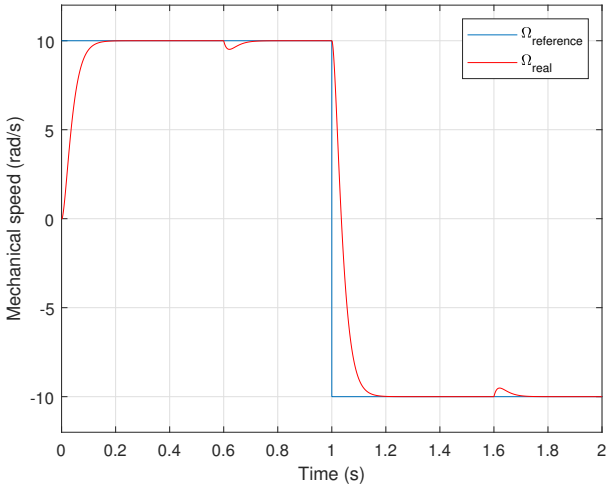

(a) Mechanical speed: conventional scheme

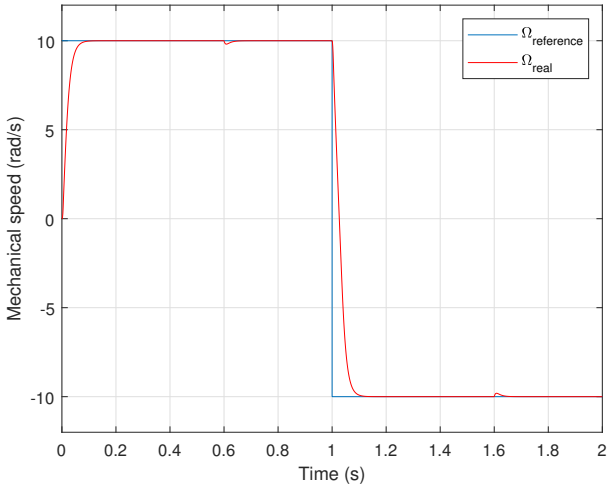

(b) Mechanical speed: proposed scheme

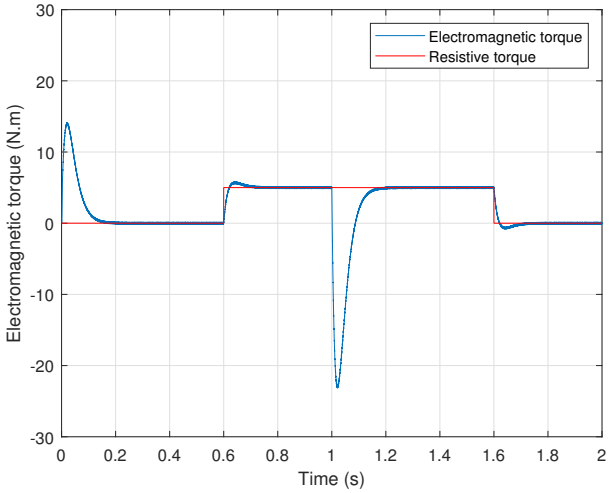

(c) Electromagnetic torque: conventional scheme

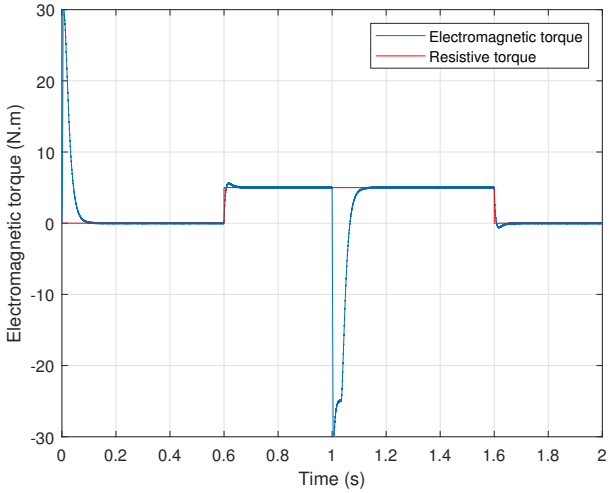

(d) Electromagnetic torque: proposed scheme

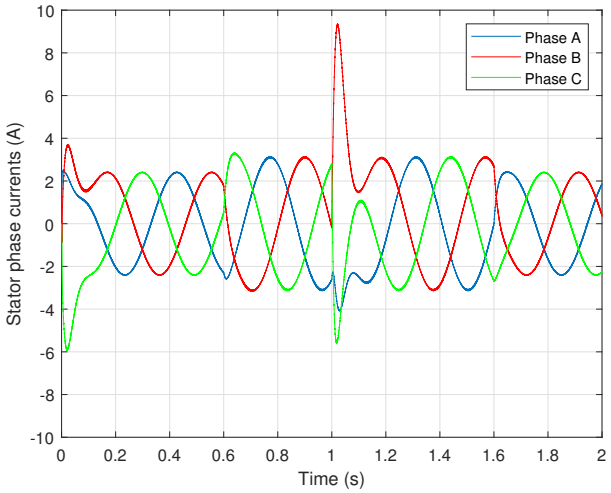

(e) Phase currents: conventional scheme

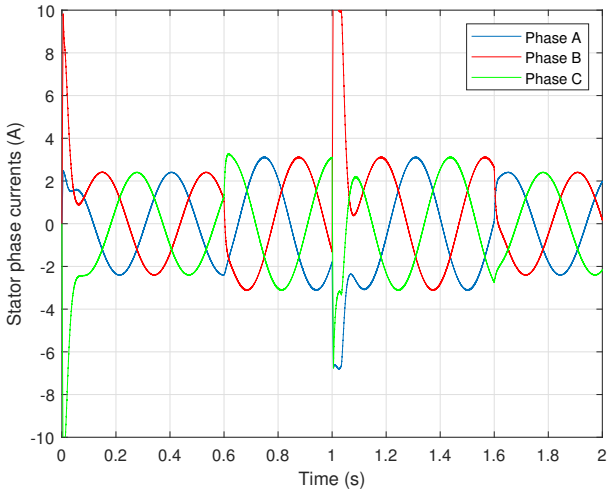

(f) Phase currents: proposed scheme

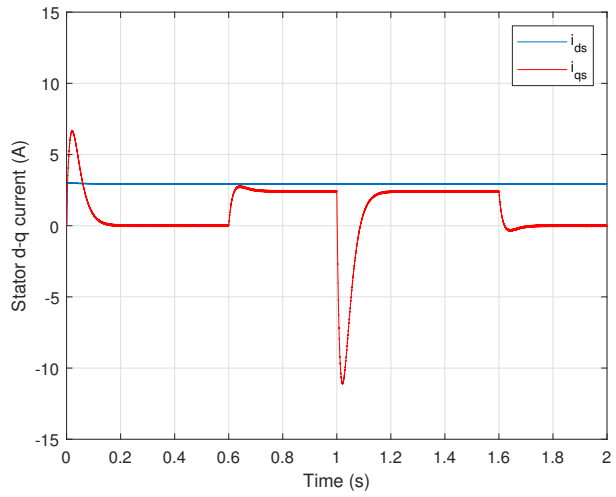

(g) d-q stator currents: conventional scheme

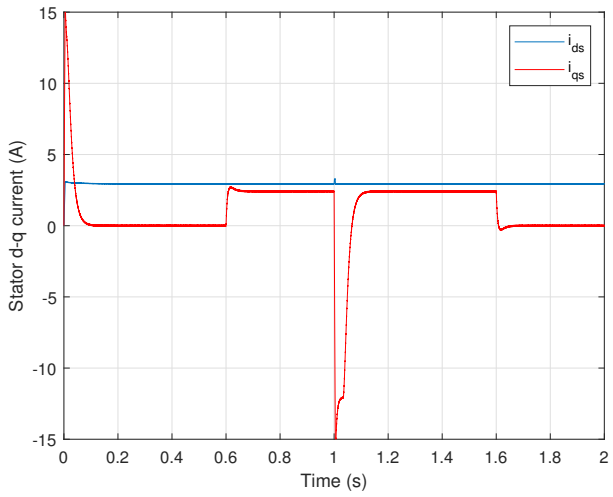

(h) d-q stator currents: proposed scheme

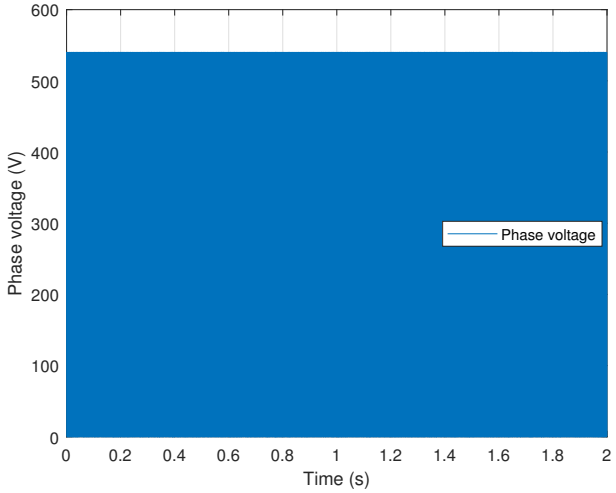

(i) Phase voltage: conventional scheme

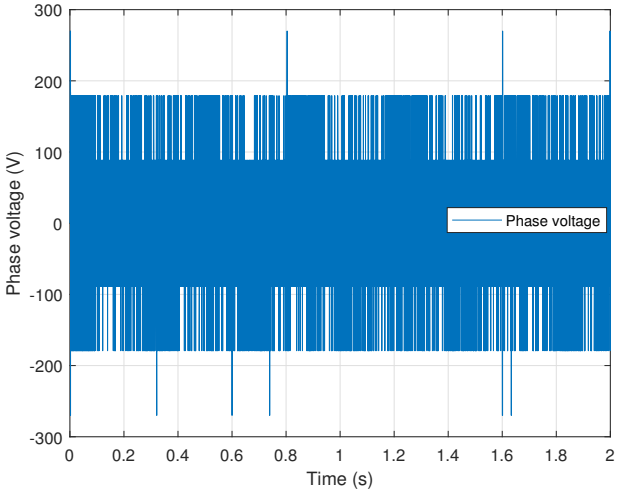

(j) Phase voltage: proposed scheme

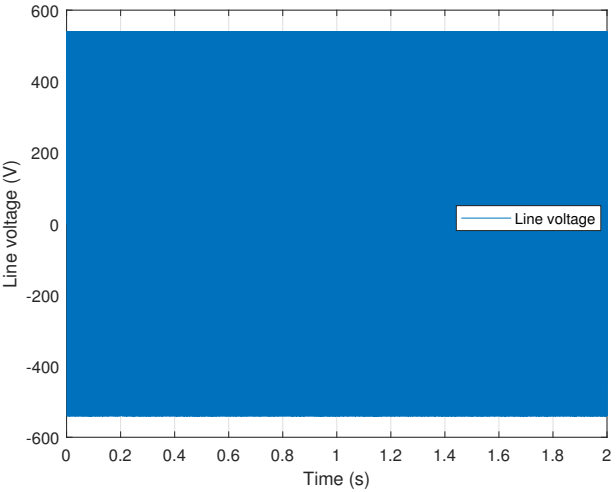

(k) Line voltage: conventional scheme

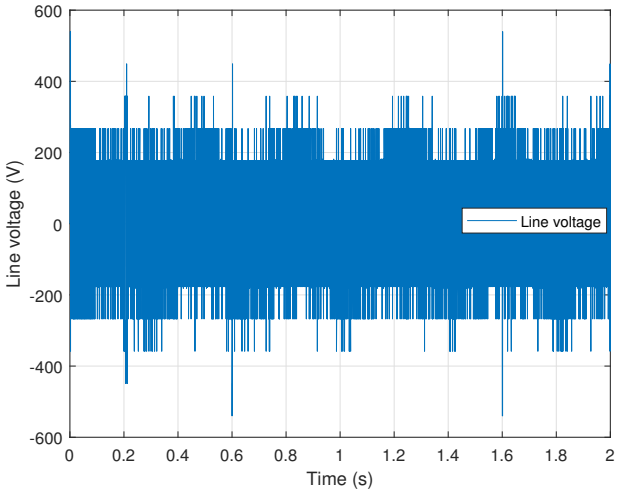

(l) Line voltage: proposed scheme

Fig. 9: Test in a low-speed region with load application

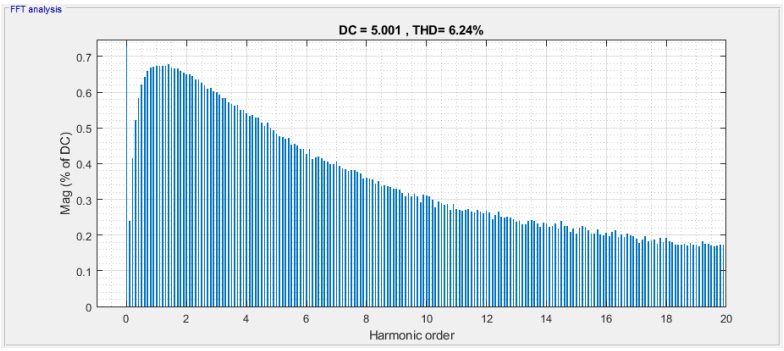

(a) Torque THD: conventional scheme

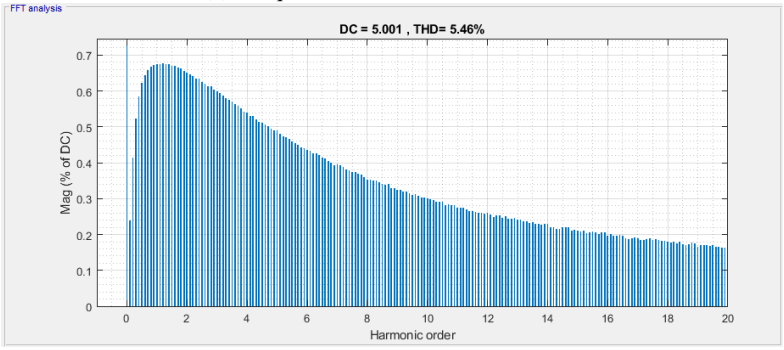

(b) Torque THD: proposed scheme

Fig. 10: Torque THD improvement

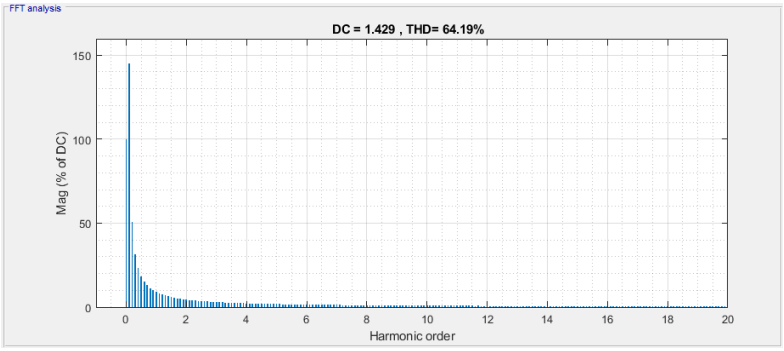

(a) Phase current THD: conventional scheme

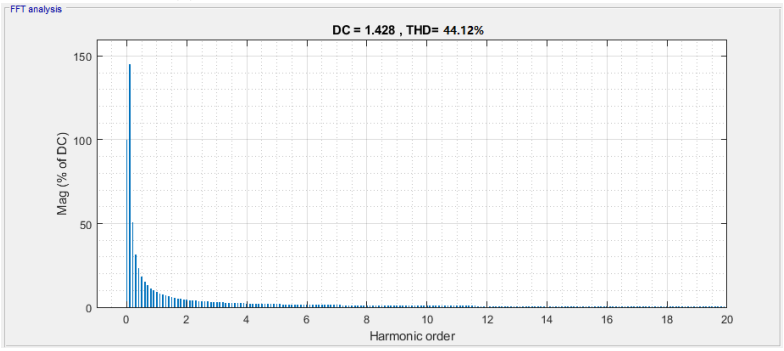

(b) Phase current THD: proposed scheme

Fig. 11: Phase current THD improvement

The phase voltage in Fig. 9(i) shows the voltage waveform on one leg of the conventional two-level inverter. Fig. 9(j) shows the voltage waveform on one leg of the proposed five-level inverter.

The line voltage in Fig. 9(k) shows the two voltage levels generated by the conventional two-level inverter. Fig. 9(l) shows the five voltage levels generated by the proposed five-level inverter.

The torque ripples have been reduced notably with the proposed multilevel inverter topology. The conventional technique has a high torque ripple level of 6.24% (Fig. 10(a)) compared to 5.46% for the five-level topology (Fig. 10(b)), with a difference of 0.78%.

The phase current ripples have also been reduced remarkably with the proposed multilevel inverter topology. The conventional technique has a high current ripple level of 64.19% (Fig. 11(a)) compared to 44.12% for the five-level topology (Fig. 11(b)), with a difference of 20.07%.

The maximum torque per ampere (MTPA) vector control strategy ensures high performance and operation dynamics, even at very low-speed regions. The key is the choice of the way the reference current values will be defined. This strategy is used mainly at start-ups and for low speeds. MTPA consists of minimizing the current for a given torque to reduce the Joule losses.

The quantity of produced torque ripples is a particularly important feature in the case of speed control applications. This is because an immoderate amount of torque ripples lead to imprecise positioning. The precision becomes significantly more difficult or even impossible. Moreover, the torque ripples can lead to resonances that can harm the mechanics.

For example, the proposed technique is suitable for more precise position control applications, conventional computer numerical control (CNC) machines, etc., while the conventional technique is suitable for simple positioning applications, simple CNC machines (i.e. the ones that use stepper motors, or brushless DC motors for positioning), etc.

VII. Conclusions

For the synchronous reluctance motor operation, a better vector control method based on the MTPA strategy and multilevel inverter architecture has been designed and simulated. Overall, the suggested method improved dynamic system performance while being run at a very low speed. The system responded quickly to an instant load application, which demonstrates faster dynamics. When compared to the conventional scheme, the proposed technique's torque pulsation and current distortion were smoother. Significantly less torque and current ripples were seen, and their waveforms were smoother. Based on the acquired results, a system developed using the suggested technique was very accurate and efficient; the performance of the enhanced system is significantly impacted by the addition of multilevel inverter topology based on alternating carriers PWM and anti-windup controllers.

This study can be developed into a reliable sensorless system. First off, switching from PI controllers to fuzzy logic controllers or sliding mode ones can be a significant deal. Second, the speed trans-coder can be replaced with an extended Kalman filter for mechanical speed observation.

References

[1] S. Chowdhury, E. Gurpinar, G.-J. Su, T. Raminosoa, T. A. Burress, and B. Ozpineci, "Enabling Technologies for Compact Integrated Electric Drives for Automotive Traction Applications," in *2019 IEEE Transportation Electrification Conference and Expo (ITEC)*, Jun. 2019, pp. 1–8.

[2] E. Agamloh, A. von Jouanne, and A. Yokochi, "An Overview of Electric Machine Trends in Modern Electric Vehicles," *Machines*, vol. 8, no. 2, p. 20, Jun. 2020.

[3] M. Murataliyev, M. Degano, M. Di Nardo, N. Bianchi, and C. Gerada, "Synchronous Reluctance Machines: A Comprehensive Review and Technology Comparison," *Proceedings of the IEEE*, vol. 110, no. 3, pp. 382–399, Mar. 2022.

[4] S. Ricci and V. Meacci, "Simple Torque Control Method for Hybrid Stepper Motors Implemented in FPGA," *Electronics*, vol. 7, no. 10, p. 242, Oct. 2018.

[5] H. Heidari, A. Rassõlkin, A. Kallaste, T. Vaimann, and E. Andriushchenko, "Vector Control Of Synchronous Reluctance Motor With Reduced Torque Ripples," in *2020 XI International Conference on Electrical Power Drive Systems (ICEPDS)*, Oct. 2020, pp. 1–5.

[6] N. G. Ozcelik, U. E. Dogru, M. Imeryuz, and L. T. Ergene, "Synchronous Reluctance Motor vs. Induction Motor at Low-Power Industrial Applications: Design and Comparison," *Energies*, vol. 12, no. 11, p. 2190, Jan. 2019.

[7] I.-Y. L. Hsieh, M. S. Pan, and W. H. Green, "Transition to electric vehicles in China: Implications for private motorization rate and battery market," *Energy Policy*, vol. 144, p. 111654, Sep. 2020.

[8] B. Souad, "Analysis of conductive and convective transfers in a double salience switched reluctance machine by analytical coupling-2D finite elements," *Serbian Journal of Electrical Engineering*, vol. 17, no. 3, pp. 377–387, 2020.

[9] C. Fahassa, Y. Zahraoui, M. Akherraz, M. Kharrich, E. E. Elattar, and S. Kamel, "Induction Motor DTC Performance Improvement by Inserting Fuzzy Logic Controllers and Twelve-Sector Neural Network Switching Table," *Mathematics*, vol. 10, no. 9, p. 1357, Jan. 2022.

[10] J. Wang, Y. Li, S. Wu, Z. Yu, and L. Chen, "Analysis of the Influence of Parameter Condition on Whole Load Power Factor and Efficiency of Line Start Permanent Magnet Assisted Synchronous Reluctance Motor," *Energies*, vol. 15, no. 11, p. 3866, Jan. 2022.

[11] S. Yammine, C. Henaux, M. Fadel, and a. F. Messine, "Torque Ripple Reduction in a SynRM at a Constant Average Torque by Means of Current Harmonics Injection," *Progress In Electromagnetics Research C*, vol. 80, pp. 167–180, 2018.

[12] F.-J. Lin, M.-S. Huang, S.-G. Chen, and C.-W. Hsu, "Intelligent Maximum Torque per Ampere Tracking Control of Synchronous Reluctance Motor Using Recurrent Legendre Fuzzy Neural Network," *IEEE Transactions on Power Electronics*, vol. 34, no. 12, pp. 12 080–12 094, Dec. 2019.

[13] D. Igrec, A. Chowdhury, B. Štumberger, and A. Sarjaš, "Robust tracking system design for a synchronous reluctance motor – SynRM based on a new modified bat optimization algorithm," *Applied Soft Computing*, vol. 69, pp. 568–584, Aug. 2018.

[14] M. N. Ibrahim, H. Rezk, M. Al-Dhaifallah, and P. Sergeant, "Solar Array Fed Synchronous Reluctance Motor Driven Water Pump: An Improved Performance Under Partial Shading Conditions," *IEEE Access*, vol. 7, pp. 77 100–77 115, 2019.

[15] G. Boztas, O. Aydogmus, M. Caner, and H. Guldemir, "Design, optimisation and implementation of low-voltage synchronous reluctance motor for solar-powered systems," *IET Power Electronics*, vol. 12, no. 7, pp. 1679–1685, 2019.

[16] H. N. Choi, J. Seong Lee, and I. H. Park, "Shape Optimization of SynRM to Obtain Minimum Torque Ripple Using Continuum Sensitivity Analysis," in *2020 23rd International Conference on Electrical Machines and Systems (ICEMS)*, Nov. 2020, pp. 1134–1137.

[17] K. B. Tawfiq, M. N. Ibrahim, E. E. El-Kholy, and P. Sergeant, "Performance Improvement of Synchronous Reluctance Machines—A Review Research," *IEEE Transactions on Magnetics*, vol. 57, no. 10, pp. 1–11, Oct. 2021.

[18] T.-H. Lee, D.-K. Lim, K.-Y. Moon, and K.-W. Jeon, "Topology Optimization Combined with a Parametric Algorithm for Industrial Synchronous Reluctance Motor Design," *Processes*, vol. 10, no. 4, p. 746, Apr. 2022.

[19] R. Rouhani, S. E. Abdollahi, and S. A. Gholamian, "Torque ripple reduction of a synchronous reluctance motor for electric vehicle applications," in *2018 9th Annual Power Electronics, Drives Systems and Technologies Conference (PEDSTC)*, Feb. 2018, pp. 386–391.

[20] Y. Zahraoui, A. Bennassar, M. Akherraz, and A. Essalmi, "Indirect vector control of induction motor using an extended Kalman observer and fuzzy logic controllers," in *2015 3rd International Renewable and Sustainable Energy Conference (IRSEC)*, Dec. 2015, pp. 1–6.

[21] N. A. Dobroskok and V. S. Lavrinovskiy, "Spectral Analysis of Basic Algorithms of Pulse-Width Modulation Control without Feedback in Two-Level Frequency Converters," *Russian Electrical Engineering*, vol. 92, no. 3, pp. 139–144, Mar. 2021.

[22] F. P. Scalcon, C. J. Volpato, T. Lazzari, T. S. Gabbi, R. P. Vieira, and H. A. Gründling, "Sensorless Control of a SynRM Drive Based on a Luenberger Observer with an Extended EMF Model," in *IECON 2019 - 45th Annual Conference of the IEEE Industrial Electronics Society*, vol. 1, Oct. 2019, pp. 1333–1338.

[23] S. Sriprang, N. Poonnoy, D. Guilbert, B. Nahid-Mobarakeh, N. Takorabet, N. Bizon, and P. Thounthong, "Design, Modeling, and Differential Flatness Based Control of Permanent Magnet-Assisted Synchronous Reluctance Motor for e-Vehicle Applications," *Sustainability*, vol. 13, no. 17, p. 9502, Jan. 2021.

[24] M. U. Naseer, A. Kallaste, B. Asad, T. Vaimann, and A. Rassõlkin, "Analytical modelling of synchronous reluctance motor including nonlinear magnetic condition," *IET Electric Power Applications*, vol. 16, no. 4, pp. 511–524, 2022.

[25] H. Mahmoud, G. Bacco, M. Degano, N. Bianchi, and C. Gerada, "Synchronous Reluctance Motor Iron Losses: Considering Machine Nonlinearity at MTPA, FW, and MTPV Operating Conditions," *IEEE Transactions on Energy Conversion*, vol. 33, no. 3, pp. 1402–1410, Sep. 2018.

[26] T. Vajsz, L. Szamel, and A. Handler, "An Investigation of Direct Torque Control and Hysteresis Current Vector Control for Motion Control Synchronous Reluctance Motor Applications," *Power Electronics and Drives*, vol. 4, no. 39, 2019.

[27] Y. I. Nadjai, H. Ahmed, N. Takorabet, and P. Haghgooei, "Maximum Torque per Ampere Control of Permanent Magnet Assisted Synchronous Reluctance Motor: An Experimental Study," *International Journal of Robotics and Control Systems*, vol. 1, no. 4, pp. 416–427, Oct. 2021.

[28] Y. Zahraoui, M. Moutchou, and S. Tayane, "Robust vector control of synchronous reluctance motor using space vector modulation algorithm," in *2022 3rd International Conference on Digital Age & Technological Advances for Sustainable Development (ICDATA)*, May 2022, pp. 1–11.

[29] F.-J. Lin, M.-S. Huang, S.-G. Chen, C.-W. Hsu, and C.-H. Liang, "Adaptive Backstepping Control for Synchronous Reluctance Motor Based on Intelligent Current Angle Control," *IEEE Transactions on Power Electronics*, vol. 35, no. 7, pp. 7465–7479, Jul. 2020.

[30] W. Zhang, F. Xiao, J. Liu, Z. Mai, and C. Li, "Maximum Torque per Ampere Control for IPMSM Traction System Based on Current Angle Signal Injection Method," *Journal of Electrical Engineering & Technology*, vol. 15, no. 4, pp. 1681–1691, Jul. 2020.

[31] W. Lee, J. Kim, P. Jang, and K. Nam, "On-Line MTPA Control Method for Synchronous Reluctance Motor," *IEEE Transactions on Industry Applications*, vol. 58, no. 1, pp. 356–364, Jan. 2022.

[32] Y. Zahraoui, M. Moutchou, and S. Tayane, "Vector Control Strategies for Synchronous Reluctance Motor: Constant Current Control, MTPA, MTPW, and MPFC," *International Journal of Modelling, Identification and Control*, vol. 38, no. 3-4, pp. 271–281, Jan. 2023.

[33] R. Krishan, K. Kumar, and R. Roy, "Comparative Analysis of Constant Torque Angle Control and Constant Mutual Flux Linkage Control of Permanent Magnet Synchronous Motor," in *2018 2nd International Conference on Power, Energy and Environment: Towards Smart Technology (ICEPE)*, Jun. 2018, pp. 1–9.

[34] B. Sarsembayev, K. Suleimenov, and T. D. Do, "High Order Disturbance Observer Based PI-PI Control System With Tracking Anti-Windup Technique for Improvement of Transient Performance of PMSM," *IEEE Access*, vol. 9, pp. 66 323–66 334, 2021, conference Name: IEEE Access.

[35] V. V. Hadke and M. P. Thakre, "Integrated Multilevel Converter Topology for Speed Control of SRM Drive in Plug in-Hybrid Electric Vehicle," in *2019 3rd International Conference on Trends in Electronics and Informatics (ICOEI)*, Apr. 2019, pp. 1013–1018.

[36] M. P. Thakre and P. S. Borse, "Analytical Evaluation of FOC and DTC Induction Motor Drives in Three Levels and Five Levels Diode Clamped Inverter," in *2020 International Conference on Power, Energy, Control and Transmission Systems (ICPECTS)*, Dec. 2020, pp. 1–6.

[37] H. Saini, S. N, A. Jakhar, and A. K. Verma, "Design and Implementation of Five Level Inverter Topology for More Electric Aircraft Application," in *2022 IEEE International Conference on Power Electronics, Smart Grid, and Renewable Energy (PESGRE)*, Jan. 2022, pp. 1–6.

[38] Y. Zahraoui, M. Akherraz, C. Fahassa, and S. Elbadaoui, "Induction Motor DTC Performance Improvement by Reducing Flux and Torque Ripples in Low Speed," *Journal of Robotics and Control (JRC)*, vol. 3, no. 1, pp. 93–100, Jan. 2022.

[39] M. Saeedian, S. M. Hosseini, and J. Adabi, "A Five-Level Step-Up Module for Multilevel Inverters: Topology, Modulation Strategy, and Implementation," *IEEE Journal of Emerging and Selected Topics in Power Electronics*, vol. 6, no. 4, pp. 2215–2226, Dec. 2018.

[40] S.-M. Kim, J.-S. Lee, and K.-B. Lee, "A Modified Level-Shifted PWM Strategy for Fault-Tolerant Cascaded Multilevel Inverters With Improved Power Distribution," *IEEE Transactions on Industrial Electronics*, vol. 63, no. 11, pp. 7264–7274, Nov. 2016, conference Name: IEEE Transactions on Industrial Electronics.

[41] O. J. Tola, E. A. Umoh, and E. A. Yahaya, "Pulse Width Modulation Analysis of Five-Level Inverter- Fed Permanent Magnet Synchronous Motors for Electric Vehicle Applications," *International Journal of Robotics and Control Systems*, vol. 1, no. 4, pp. 477–487, Nov. 2021.

[42] J. Chen, C. Wang, and J. Li, "Single-Phase Step-Up Five-Level Inverter with Phase-Shifted Pulse Width Modulation," *Journal of Power Electronics*, vol. 19, no. 1, pp. 134–145, 2019.